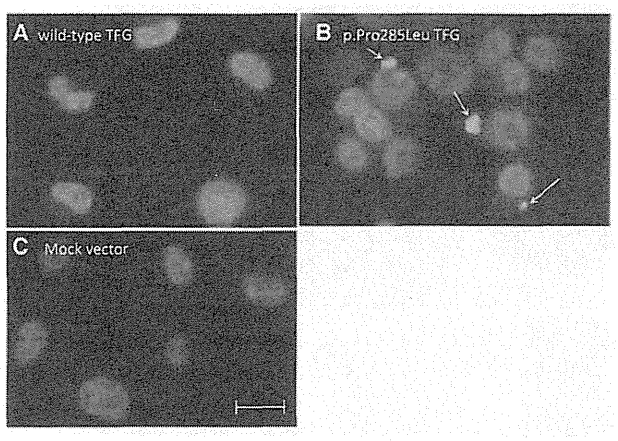

Figure 5. Formation of Cytoplasmic TDP-43 Aggregation Bodies in Cells Stably Expressing Mutant p.Pro285Leu TFG
The coding sequence of *TFG* cDNA was subcloned into pBluescript (Stratagene). After site-directed mutagenesis with a primer pair shown in Table S9, the mutant cDNAs were cloned into the BamHI and XhoI sites of pcDNA3 (Life Technologies). Stable cell lines were established by Lipofectamine (Life Technologies) transfection according to the manufacturer's instructions. Established cell lines were cultured under the ordinary cell-culture conditions (37°C and 5% CO_2) for 5–6 days and were subjected to immunocytochemical analyses. Neuro-2a cells stably expressing wild-type TFG (A), mutant TFG (p.Pro285Leu) (B), and a mock vector (C) are shown. TDP-43-immunopositive cytoplasmic inclusions are absent in the cells stably expressing wild-type TFG or the mock vector (A and C); however, TDP-43-immunopositive cytoplasmic inclusions were exclusively demonstrated in cells stably expressing mutant TFG (p.Pro285Leu), as indicated by arrows (B). Similar results were obtained with HEK 293 cells (not shown). Scale bars represent 10 μm.

a TGN46 antibody. It revealed that the Golgi apparatus was fragmented in approximately 70% of the remaining motor neurons in the lumbar anterior horn. The fragmentation of the Golgi apparatus was prominent near TFG-positive inclusion bodies (Figures 4N–4R). In summary, we found abnormal TDP-43-immunopositive inclusions in the cytoplasm of motor neurons, as well as fragmentation of the Golgi apparatus in HMSN-P, confirming the overlapping neuropathological features between HMSN-P and sporadic ALS.

To further investigate the effect of mutant TFG in cultured cells, stable cell lines expressing wild-type and mutant TFG (p.Pro285Leu) were established from neuro-2a and human embryonic kidney (HEK) 293 cells as previously described.[18] Established cell lines were cultured under the ordinary cell-culture conditions (37°C and 5% CO_2) for 5–6 days and were subjected to immunocytochemical analyses. The neuro-2a cells stably expressing wild-type or mutant TFG demonstrated no distinct difference in the distribution of endogenous TFG, FUS, or OPTN (data not shown). In contrast, cytoplasmic inclusions containing endogenous TDP-43 were exclusively observed in the neuro-2a cells stably expressing untagged mutant TFG, but not in those expressing wild-type TFG (Figure 5). Similar data were obtained from HEK 293 cells (data not shown). Thus, the expression of mutant TFG leads to mislocalization and inclusion-body formation of TDP-43 in cultured cells.

TFG was originally identified as a part of fusion oncoproteins (NTRK1-T3 in papillary thyroid carcinoma,[19] TFG-ALK in anaplastic large cell lymphoma,[20] and TFG/NOR1 in extraskeletal myxoid chondrosarcoma[21]), where the N-terminal portions of TFG are fused to the C terminus of tyrosine kinases or a superfamily of steroid-thyroid hormone-retinoid receptors acting as a transcriptional activator leading to the formation of oncogenic products. Very recently, TFG-1, a homolog of TFG in *Caenorhabditis elegans*, and TFG have been discovered to localize in endoplasmic-reticulum exit sites. TFG-1 acts in a hexameric form that binds the scaffolding protein Sec16 complex assembly and plays an important role in protein secretion with COPII-coated vesicles.[22] It is noteworthy that mutations in genes involved in vesicle trafficking[23,24] (such genes include *VAPB*, *CHMP2B*, *alsin*, *FIG4*, *VPS33B*, *PIP5K1C*, and *ERBB3*) cause motor neuron diseases, emphasizing the role of vesicle trafficking in motor neuron diseases. Thus, altered vesicle trafficking due to the *TFG* mutation might be involved in the motor neuron degeneration in HMSN-P. The presence of TFG-immunopositive inclusions in motor neurons raises the possibility that mutant TFG results in the misfolding and formation of cytoplasmic aggregate bodies, as well as altered vesicle trafficking.

An intriguing neuropathological finding is TDP-43-positive cytoplasmic inclusions in the motor neurons; these inclusions have recently been established as the fundamental neuropathological findings in ALS.[13,14] Of note, expression of mutant, but not wild-type, TFG in cultured cells led to the formation of TDP-43-containing cytoplasmic aggregation. These observations are similar

(M–M″) An inclusion immunopositive for both TFG (green) and TDP-43 (red) is observed in a small number of neurons. The scale bars represent 20 μm.
(N) Normal Golgi apparatus in the neurons of the intact thoracic intermediolateral nucleus. The scale bar represents 20 μm.
(O and P) Fragmentation of the Golgi apparatus with small, round, and disconnected profiles in the affected motor neurons of the lumbar anterior horn. The scale bars represent 20 μm.
(Q–R″) Immunohistochemical observations of the Golgi apparatus and TFG-immunopositive inclusions employing antibodies against TGN46 (red) and TFG (green), respectively. The scale bars represent 10 μm.
(Q) Normal size and distribution (red) in a motor neuron without inclusions.
(R–R″) The Golgi apparatus was fragmented into various sizes and reduced in number in the lumbar anterior horn motor neuron with TFG-positive inclusions (green). The fragmentation predominates near the inclusion (arrow), whereas the Golgi apparatuses distant from the inclusion showed nearly normal patterns (arrow head).

to what has been described for ALS, where TDP-43 is mislocalized from the normally localized nucleus to the cytoplasm with concomitant cytoplasmic inclusions. Cytoplasmic TDP-43 accumulation and inclusion formation have also been observed in motor neurons in familial ALS with mutations in *VAPB* (MIM 608627) or *CHMP2B* (MIM 600795).[25,26] Furthermore, TDP-43 pathology has been demonstrated in transgenic mice expressing mutant VAPB.[27] Although the mechanisms of mislocalization of TDP-43 remain to be elucidated, these observations suggest connections between alteration of vesicle trafficking and mislocalization of TDP-43. Thus, common pathophysiologic mechanisms might underlie motor neuron degenerations involving vesicle trafficking including TFG, as well as VAPB and CHMP2B. Because TDP-43 is an RNA-binding protein, RNA dysregulation has been suggested to play important roles in the TDP43-mediated neurodegeneration.[28] Furthermore, recent discovery of hexanucleotide repeat expansions in *C9ORF72* in familial and sporadic ALS/FTD (MIM 105550)[29,30] emphasizes the RNA-mediated toxicities as the causal mechanisms of neurodegeneration. Observations of TDP-43-positive cytoplasmic inclusions in the motor neurons of the patient with HMSN-P raise the possibility that RNA-mediated mechanisms might also be involved in motor neuron degeneration in HMSN-P.

In summary, we have found that *TFG* mutations cause HMSN-P. The presence of TFG/ubiquitin- and/or TDP-43-immunopositive cytoplasmic inclusions in motor neurons and cytosolic aggregation composed of TDP-43 in cultured cells expressing mutant TFG indicate a novel pathway of motor neuron death.

Supplemental Data

Supplemental Data include three figures and nine tables and can be found with this article online at http://www.cell.com/AJHG/.

Acknowledgments

The authors thank the families for participating in the study. We also thank the doctors who obtained clinical information of the patients. This work was supported in part by Grants-in-Aid for Scientific Research on Innovative Areas (22129002); the Global Centers of Excellence Program; the Integrated Database Project; Scientific Research (A) (B21406026) and Challenging Exploratory Research (23659458) from the Ministry of Education, Culture, Sports, Science, and Technology of Japan; a Grant-in-Aid for Research on Intractable Diseases and Comprehensive Research on Disability Health and Welfare from the Ministry of Health, Labour, and Welfare, Japan; Grants-in-Aid from the Research Committee of CNS Degenerative Diseases; the Ministry of Health, Labour, and Welfare of Japan; the Charcot-Marie-Tooth Association; and the National Medical Research Council of Australia. H.I. was supported by a Research Fellowship from the Japan Society for the Promotion of Science for Young Scientists. We also thank S. Ogawa (Cancer Genomics Project, The University of Tokyo) for his kind help in the analyses employing GAIIx and SOLiD4.

Received: April 16, 2012
Revised: May 27, 2012
Accepted: July 2, 2012
Published online: August 9, 2012

Web Resources

The URLs for data presented herein are as follows.

1000 Genomes Project Database, http://www.1000genomes.org/
dbSNP, http://www.ncbi.nlm.nih.gov/projects/SNP/
HapMap, http://hapmap.ncbi.nlm.nih.gov/
NHLBI GO Exome Sequencing Project, https://esp.gs.washington.edu/drupal/
Online Mendelian Inheritance in Man (OMIM), http://www.omim.org
PolyPhen, http://genetics.bwh.harvard.edu/pph/
RefSeq, http://www.ncbi.nlm.nih.gov/projects/RefSeq/
UCSC Human Genome Browser, http://genome.ucsc.edu/

References

1. Takashima, H., Nakagawa, M., Nakahara, K., Suehara, M., Matsuzaki, T., Higuchi, I., Higa, H., Arimura, K., Iwamasa, T., Izumo, S., and Osame, M. (1997). A new type of hereditary motor and sensory neuropathy linked to chromosome 3. Ann. Neurol. *41*, 771–780.
2. Nakagawa, M. (2009). [Wide spectrum of hereditary motor sensory neuropathy (HMSN)]. Rinsho Shinkeigaku *49*, 950–952.
3. Maeda, K., Sugiura, M., Kato, H., Sanada, M., Kawai, H., and Yasuda, H. (2007). Hereditary motor and sensory neuropathy (proximal dominant form, HMSN-P) among Brazilians of Japanese ancestry. Clin. Neurol. Neurosurg. *109*, 830–832.
4. Patroclo, C.B., Lino, A.M., Marchiori, P.E., Brotto, M.W., and Hirata, M.T. (2009). Autosomal dominant HMSN with proximal involvement: new Brazilian cases. Arq. Neuropsiquiatr. *67* (3B), 892–896.
5. Fujita, K., Yoshida, M., Sako, W., Maeda, K., Hashizume, Y., Goto, S., Sobue, G., Izumi, Y., and Kaji, R. (2011). Brainstem and spinal cord motor neuron involvement with optineurin inclusions in proximal-dominant hereditary motor and sensory neuropathy. J. Neurol. Neurosurg. Psychiatry *82*, 1402–1403.
6. Takahashi, H., Makifuchi, T., Nakano, R., Sato, S., Inuzuka, T., Sakimura, K., Mishina, M., Honma, Y., Tsuji, S., and Ikuta, F. (1994). Familial amyotrophic lateral sclerosis with a mutation in the Cu/Zn superoxide dismutase gene. Acta Neuropathol. *88*, 185–188.
7. Maeda, K., Kaji, R., Yasuno, K., Jambaldorj, J., Nodera, H., Takashima, H., Nakagawa, M., Makino, S., and Tamiya, G. (2007). Refinement of a locus for autosomal dominant hereditary motor and sensory neuropathy with proximal dominancy (HMSN-P) and genetic heterogeneity. J. Hum. Genet. *52*, 907–914.
8. Fukuda, Y., Nakahara, Y., Date, H., Takahashi, Y., Goto, J., Miyashita, A., Kuwano, R., Adachi, H., Nakamura, E., and Tsuji, S. (2009). SNP HiTLink: A high-throughput linkage analysis system employing dense SNP data. BMC Bioinformatics *10*, 121.
9. Gudbjartsson, D.F., Thorvaldsson, T., Kong, A., Gunnarsson, G., and Ingolfsdottir, A. (2005). Allegro version 2. Nat. Genet. *37*, 1015–1016.

10. Li, H., and Durbin, R. (2009). Fast and accurate short read alignment with Burrows-Wheeler transform. Bioinformatics *25*, 1754–1760.
11. Li, H., Handsaker, B., Wysoker, A., Fennell, T., Ruan, J., Homer, N., Marth, G., Abecasis, G., and Durbin, R.; 1000 Genome Project Data Processing Subgroup. (2009). The Sequence Alignment/Map format and SAMtools. Bioinformatics *25*, 2078–2079.
12. Robinson, J.T., Thorvaldsdóttir, H., Winckler, W., Guttman, M., Lander, E.S., Getz, G., and Mesirov, J.P. (2011). Integrative genomics viewer. Nat. Biotechnol. *29*, 24–26.
13. Neumann, M., Sampathu, D.M., Kwong, L.K., Truax, A.C., Micsenyi, M.C., Chou, T.T., Bruce, J., Schuck, T., Grossman, M., Clark, C.M., et al. (2006). Ubiquitinated TDP-43 in frontotemporal lobar degeneration and amyotrophic lateral sclerosis. Science *314*, 130–133.
14. Arai, T., Hasegawa, M., Akiyama, H., Ikeda, K., Nonaka, T., Mori, H., Mann, D., Tsuchiya, K., Yoshida, M., Hashizume, Y., and Oda, T. (2006). TDP-43 is a component of ubiquitin-positive tau-negative inclusions in frontotemporal lobar degeneration and amyotrophic lateral sclerosis. Biochem. Biophys. Res. Commun. *351*, 602–611.
15. Hasegawa, M., Arai, T., Nonaka, T., Kametani, F., Yoshida, M., Hashizume, Y., Beach, T.G., Buratti, E., Baralle, F., Morita, M., et al. (2008). Phosphorylated TDP-43 in frontotemporal lobar degeneration and amyotrophic lateral sclerosis. Ann. Neurol. *64*, 60–70.
16. Inukai, Y., Nonaka, T., Arai, T., Yoshida, M., Hashizume, Y., Beach, T.G., Buratti, E., Baralle, F.E., Akiyama, H., Hisanaga, S., and Hasegawa, M. (2008). Abnormal phosphorylation of Ser409/410 of TDP-43 in FTLD-U and ALS. FEBS Lett. *582*, 2899–2904.
17. Stieber, A., Chen, Y., Wei, S., Mourelatos, Z., Gonatas, J., Okamoto, K., and Gonatas, N.K. (1998). The fragmented neuronal Golgi apparatus in amyotrophic lateral sclerosis includes the trans-Golgi-network: Functional implications. Acta Neuropathol. *95*, 245–253.
18. Kuroda, Y., Sako, W., Goto, S., Sawada, T., Uchida, D., Izumi, Y., Takahashi, T., Kagawa, N., Matsumoto, M., Matsumoto, M., et al. (2012). Parkin interacts with Klokin1 for mitochondrial import and maintenance of membrane potential. Hum. Mol. Genet. *21*, 991–1003.
19. Greco, A., Mariani, C., Miranda, C., Lupas, A., Pagliardini, S., Pomati, M., and Pierotti, M.A. (1995). The DNA rearrangement that generates the TRK-T3 oncogene involves a novel gene on chromosome 3 whose product has a potential coiled-coil domain. Mol. Cell. Biol. *15*, 6118–6127.
20. Hernández, L., Pinyol, M., Hernández, S., Beà, S., Pulford, K., Rosenwald, A., Lamant, L., Falini, B., Ott, G., Mason, D.Y., et al. (1999). TRK-fused gene (TFG) is a new partner of ALK in anaplastic large cell lymphoma producing two structurally different TFG-ALK translocations. Blood *94*, 3265–3268.
21. Hisaoka, M., Ishida, T., Imamura, T., and Hashimoto, H. (2004). TFG is a novel fusion partner of NOR1 in extraskeletal myxoid chondrosarcoma. Genes Chromosomes Cancer *40*, 325–328.
22. Witte, K., Schuh, A.L., Hegermann, J., Sarkeshik, A., Mayers, J.R., Schwarze, K., Yates, J.R., 3rd, Eimer, S., and Audhya, A. (2011). TFG-1 function in protein secretion and oncogenesis. Nat. Cell Biol. *13*, 550–558.
23. Dion, P.A., Daoud, H., and Rouleau, G.A. (2009). Genetics of motor neuron disorders: New insights into pathogenic mechanisms. Nat. Rev. Genet. *10*, 769–782.
24. Andersen, P.M., and Al-Chalabi, A. (2011). Clinical genetics of amyotrophic lateral sclerosis: What do we really know? Nat Rev Neurol *7*, 603–615.
25. Ince, P.G., Highley, J.R., Kirby, J., Wharton, S.B., Takahashi, H., Strong, M.J., and Shaw, P.J. (2011). Molecular pathology and genetic advances in amyotrophic lateral sclerosis: an emerging molecular pathway and the significance of glial pathology. Acta Neuropathol. *122*, 657–671.
26. Cox, L.E., Ferraiuolo, L., Goodall, E.F., Heath, P.R., Higginbottom, A., Mortiboys, H., Hollinger, H.C., Hartley, J.A., Brockington, A., Burness, C.E., et al. (2010). Mutations in CHMP2B in lower motor neuron predominant amyotrophic lateral sclerosis (ALS). PLoS ONE *5*, e9872.
27. Tudor, E.L., Galtrey, C.M., Perkinton, M.S., Lau, K.-F., De Vos, K.J., Mitchell, J.C., Ackerley, S., Hortobágyi, T., Vámos, E., Leigh, P.N., et al. (2010). Amyotrophic lateral sclerosis mutant vesicle-associated membrane protein-associated protein-B transgenic mice develop TAR-DNA-binding protein-43 pathology. Neuroscience *167*, 774–785.
28. Lee, E.B., Lee, V.M., and Trojanowski, J.Q. (2012). Gains or losses: Molecular mechanisms of TDP43-mediated neurodegeneration. Nat. Rev. Neurosci. *13*, 38–50.
29. DeJesus-Hernandez, M., Mackenzie, I.R., Boeve, B.F., Boxer, A.L., Baker, M., Rutherford, N.J., Nicholson, A.M., Finch, N.A., Flynn, H., Adamson, J., et al. (2011). Expanded GGGGCC hexanucleotide repeat in noncoding region of C9ORF72 causes chromosome 9p-linked FTD and ALS. Neuron *72*, 245–256.
30. Renton, A.E., Majounie, E., Waite, A., Simón-Sánchez, J., Rollinson, S., Gibbs, J.R., Schymick, J.C., Laaksovirta, H., van Swieten, J.C., Myllykangas, L., et al; ITALSGEN Consortium. (2011). A hexanucleotide repeat expansion in C9ORF72 is the cause of chromosome 9p21-linked ALS-FTD. Neuron *72*, 257–268.

The American Journal of Human Genetics, Volume *91*

Supplemental Data

The TRK-Fused Gene Is Mutated in Hereditary Motor and Sensory Neuropathy with Proximal Dominant Involvement

Hiroyuki Ishiura, Wataru Sako, Mari Yoshida, Toshitaka Kawarai, Osamu Tanabe, Jun Goto, Yuji Takahashi, Hidetoshi Date, Jun Mitsui, Budrul Ahsan, Yaeko Ichikawa, Atsushi Iwata, Hiide Yoshino, Yuishin Izumi, Koji Fujita, Kouji Maeda, Satoshi Goto, Hidetaka Koizumi, Ryoma Morigaki, Masako Ikemura, Naoko Yamauchi, Shigeo Murayama, Garth A. Nicholson, Hidefumi Ito, Gen Sobue, Masanori Nakagawa, Ryuji Kaji, and Shoji Tsuji

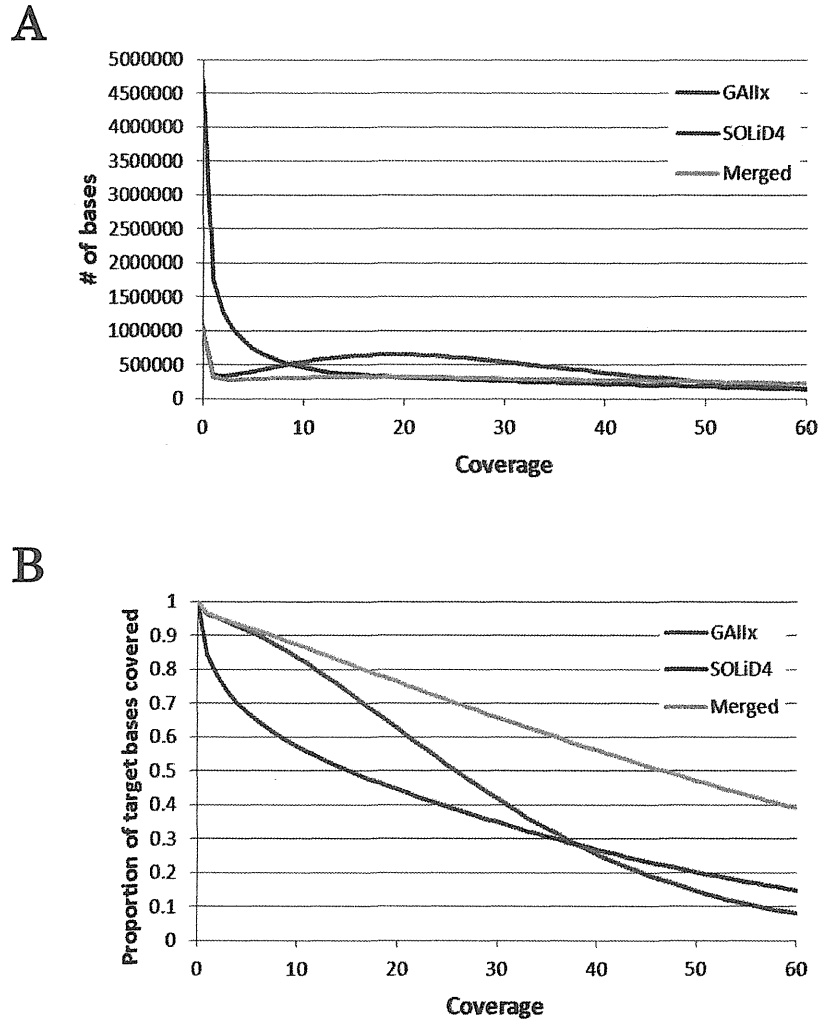

Figure S1. Coverages of Exome Analysis by GAIIx and SOLiD4

Distribution of number of bases (A) and proportion of covered target bases (B) obtained by GAIIx, SOLiD4, and merged data. Regions with capture probes +/- 10 bp are considered as target regions. 87.3% of target regions were covered by 10X or more coverage.

A

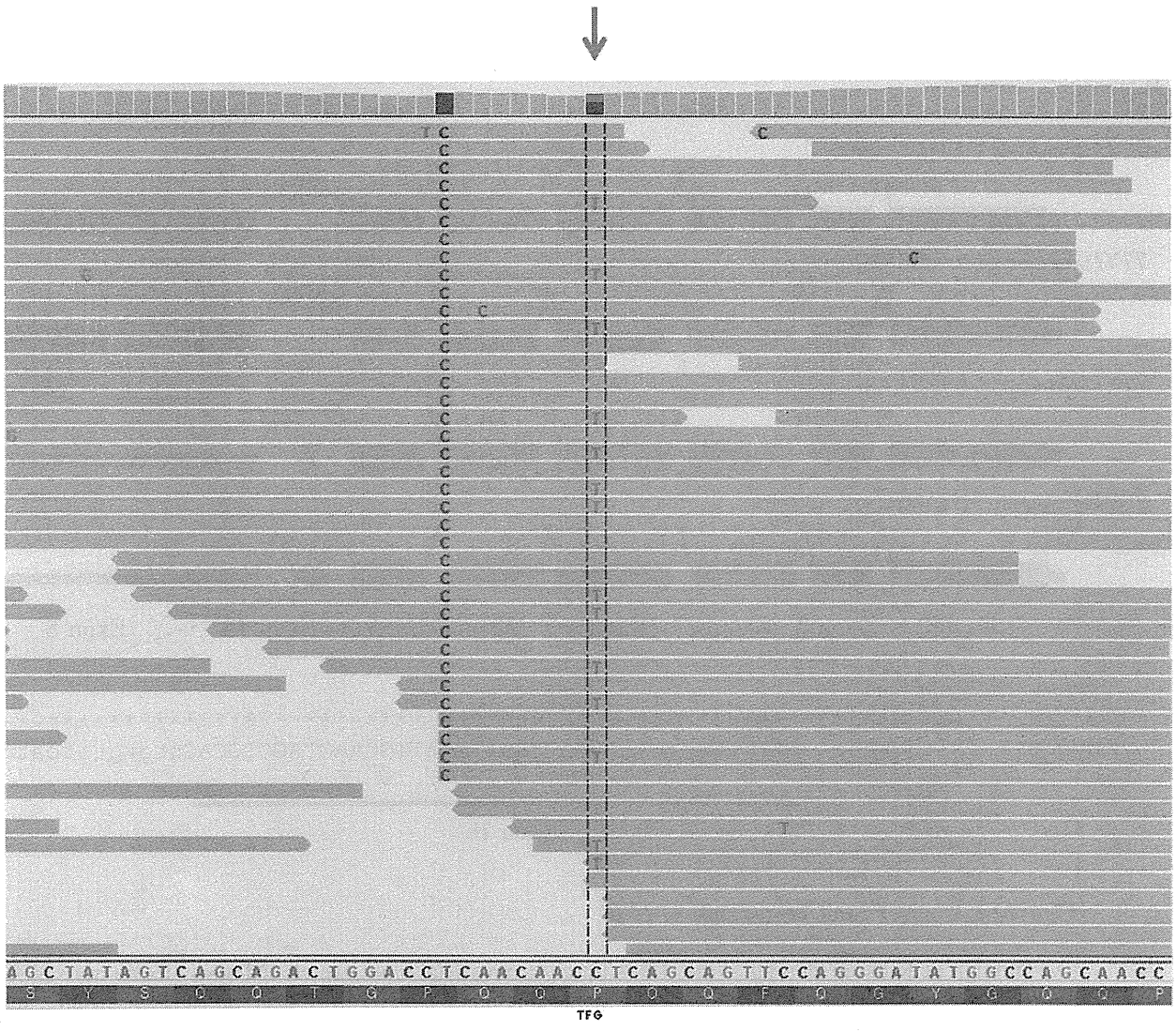

B

	Variant (T)	Reference (C)	Total
GAIIx	13	19	32
SOLiD4	3	8	11
Merged	16	27	43

Figure S2. Heterozygous *TFG* Mutation Identified as the Cause of HMSN-P

(A) Short read sequences aligned to hg18 are viewed using Integrative Genomic Viewer. The mutation in *TFG* (c.854C>T) is indicated by the red arrow. There are 27 reads corresponding to the reference base (C) and 16 reads corresponding to the variant base (T). Shown on the left (c.846T>C) is a known homozygous synonymous SNP (rs11353).

(B) Numbers of reads corresponding to the reference base and variant base are summarized.

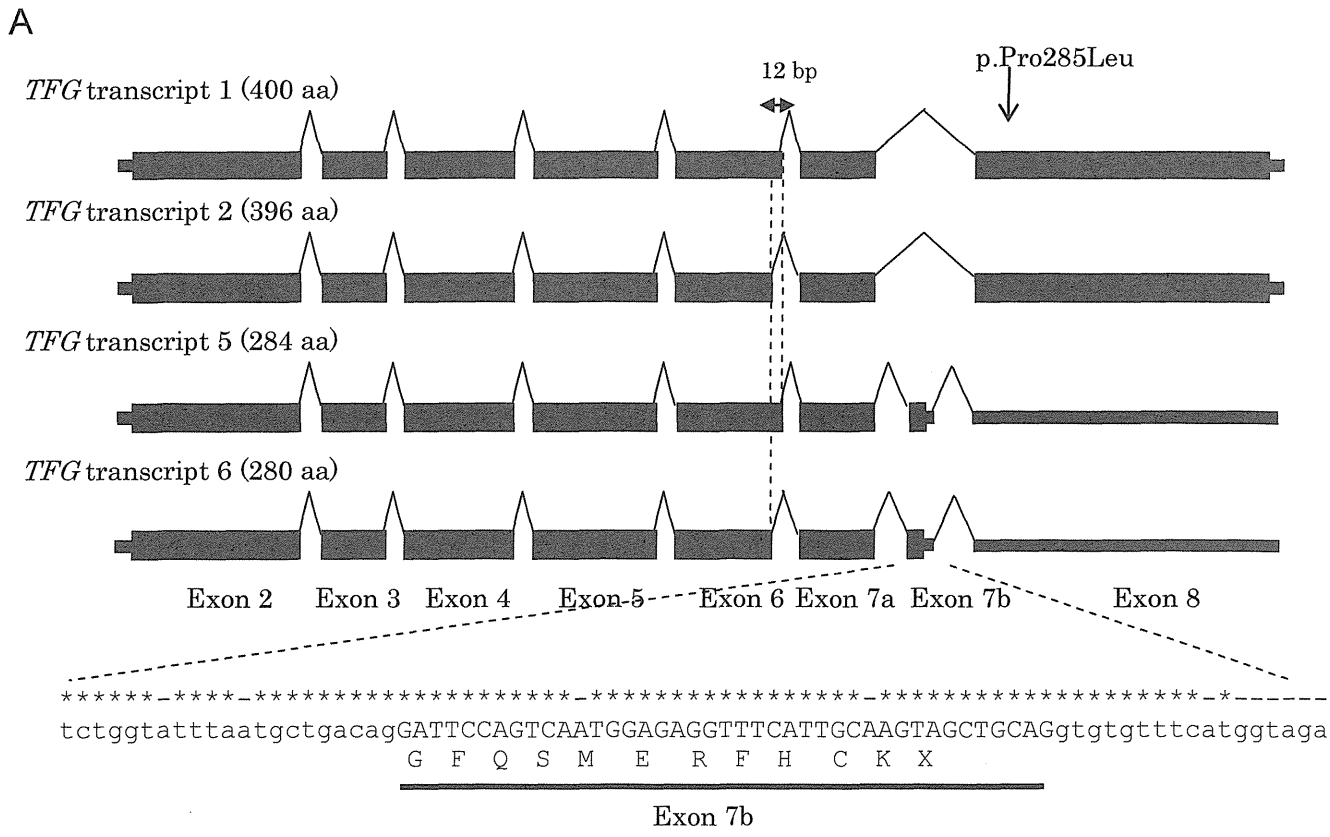

Figure S3. Newly Found Transcripts of *TFG*

(A) Through PCR-based cloning of the cDNA library from a fetal brain, we cloned newly found transcripts 5 (AB731569) and 6 (AB731570). Schematic representation of *TFG* transcripts is shown. Transcripts 2 and 6 have shorter (12 bp) exon 6 compared with transcripts 1 and 5, respectively. The exon-intron boundary and predicted amino acids of newly found exon 7b, which is included in transcripts 5 and 6, are shown below. The sequence is highly conserved among species; nucleotides marked with "*" are the nucleotides conserved among humans, rhesus monkeys, mice, dogs, elephants, opposums, and chickens.

B

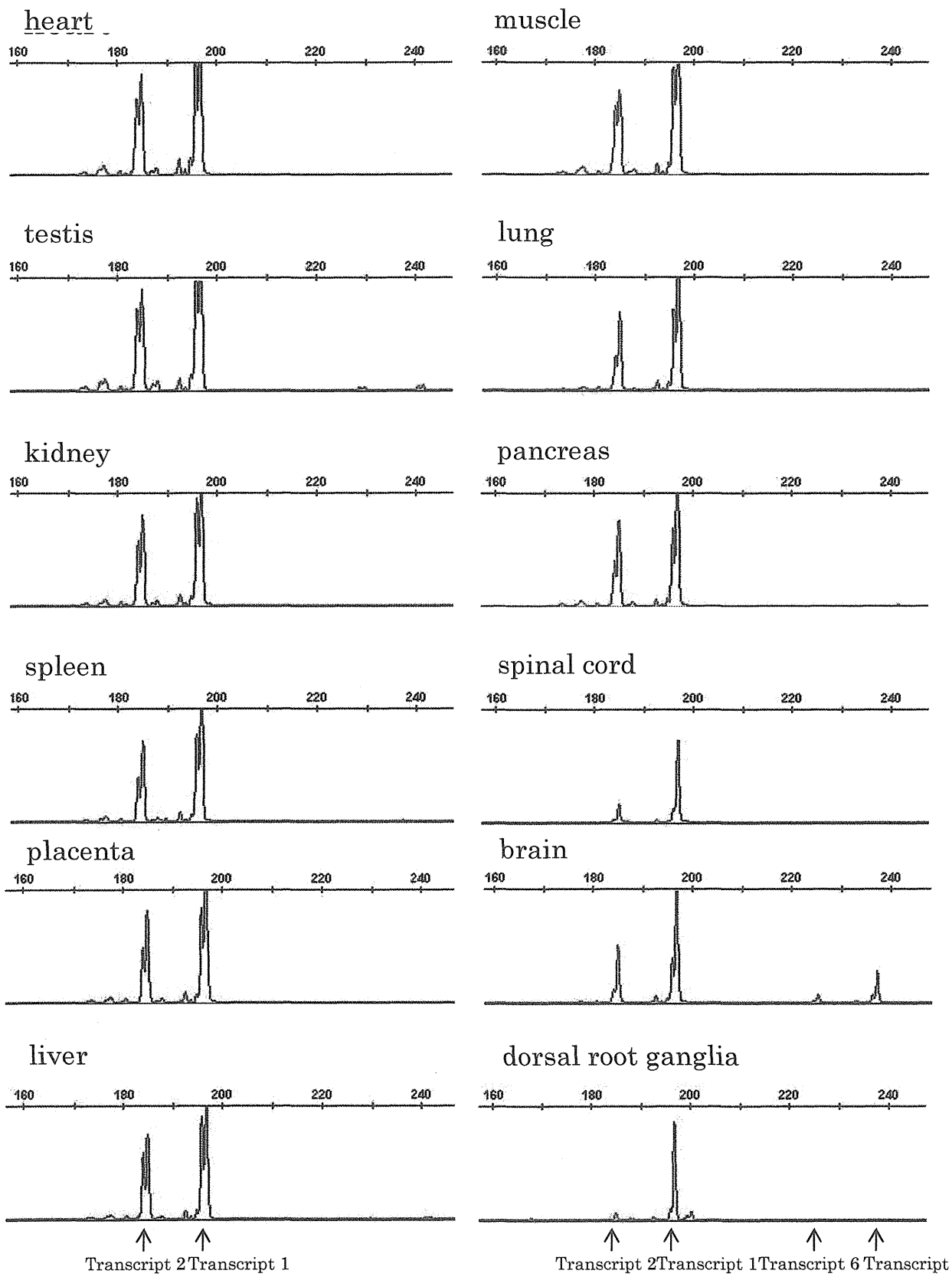

(B) RT-PCR analysis of control tissues. cDNA libraries of the heart, skeletal muscle, testis, lung, kidney, liver, pancreas, spleen, placenta, and brain were obtained from Clontech. cDNA of the spinal cord and dorsal root ganglia were prepared from a neurologically normal control. Transcripts 1, 2, 5, and 6 correspond to 196, 184, 237, and 225 bp, respectively. In neural tissues (brain, spinal cord, and dorsal root ganglia), transcript 1 is predominantly expressed.

Table S1. Electrophysiological Studies in HMSN-P Patients

	Family	Family 1	Family 2	Family 3	Family 4
	Patient ID	IV-25	V-2	III-12	III-4
	Age at examination (y)	65	53	54	54
Motor Nerve Conduction Study					
Median nerve					
	Amplitude (mV)	5.1	1.6	10.6	9.5
	Velocity (m/s)	56.1	57.0	65.2	53.7
	Distal latency (msec)	4.0	4.1	3.0	3.5
	F-wave occurrence	25%	15%	19%	18%
Ulnar nerve					
	Amplitude (mV)	n/e	n/e	13.4	6.3
	Velocity (m/s)	n/e	n/e	62.7	58.8
	Distal latency (msec)	n/e	n/e	2.8	2.6
Tibial nerve					
	Amplitude (mV)	1.1	2.1	2.0	1.6
	Velocity (m/s)	43.5	59.0	51.0	51.1
	Distal latency (msec)	4.3	3.8	4.0	4.0
	F-wave occurrence	98%	90%	94%	62%
Peroneal nerve					
	Amplitude (mV)	n/e	n/e	1.8	1.8
	Velocity (m/s)	n/e	n/e	40.6	43.8
	Distal latency (msec)	n/e	n/e	4.5	4.5
Sensory Nerve Conduction Study					
Median nerve					
	Amplitude (mV)	n/e	n/e	4.8	0.59
	Velocity (m/s)	n/e	n/e	61.0	56.4
	Distal latency (msec)	n/e	n/e	2.7	2.3
Ulnar nerve					
	Amplitude (mV)	n/e	n/e	2.7	n/d
	Velocity (m/s)	n/e	n/e	58.3	n/a
	Distal latency (msec)	n/e	n/e	2.3	n/a
Sural nerve					
	Amplitude (mV)	n/d	n/d	1.3	0.62
	Velocity (m/s)	n/a	n/a	60.4	54.0
	Distal latency (msec)	n/a	n/a	3.2	2.8

Somatosensory evoked potentials					
Median nerve					
	Erb (ms)	n/e	n/e	8.2	n/e
	N11 (ms)	n/e	n/e	10.0	n/e
	N13 (ms)	n/e	n/e	12.4	n/e
	N20 (ms)	n/e	n/e	18.2	n/e
Tibal nerve					
	P15 (ms)	n/e	n/e	n/d	n/d
	N21 (ms)	n/e	n/e	n/d	n/d
	N30 (ms)	n/d	n/d	n/d	n/d
	P38 (ms)	n/d	43.9	39.1	48.4

n/a: not attainable, n/e: not examined, n/d: not detected

Table S2. Primer Sequences Used for Genotyping of Microsatellite Markers

	Forward	Reverse
MS1	5'-GACCCACAATCCCTTTGATG-3'	5'-CGTTTCTTTCTGTGTCTGGG-3'
MS2	5'-GCAGGGAGAATTGCTTGAAC-3'	5'- ACGAATTGACCTGGAAGTGG-3'

*MS1, chr3:101,901,207-101,901,249 and MS2, chr3:102,157,749-102,157,795 in hg18

Table S3. Number of Short Reads Obtained by GAIIx and SOLiD4

	Illumina		SOLiD	
# of total reads	32,636,077		133,891,869	
Average coverage	29.0X		26.8X	
	without tag (100 bp)	tag removed (80 bp)	without tag (50 bp)	tag removed (28 bp)
# of reads	17,579,328	15,056,749	90,649,530	43,242,339
# of reads mapped	16,240,348	13,241,991	46,415,398	24,745,577
% of reads mapped	92.3%	87.9%	51.2%	57.2%
# of uniquely mapped reads	15,748,643	12,772,410	44,168,495	22,720,398
% of uniquely mapped reads	89.6%	84.8%	48.7%	52.5%

Tag sequence (20 bases) for 454 sequencer was removed prior to alignment.
Uniquely mapped reads are those that have mapping quality of >0.

Table S4. Primer Sequences Used for Direct Nucleotide Sequence Analysis of *TFG*

	Forward	Reverse
TFG exon 1	5'-aaacggaaatacccgctttc-3'	5'-ctcctagtctcccggcctc-3'
TFG exon 2	5'-tggggataatgaatcttttgg-3'	5'-ggagtttgaggtgacactgagc-3'
TFG exon 3	5'-ggtttctatgggagagtccaac-3'	5'-aaacaactacctgaacacaaataaatg-3'
TFG exon 4	5'-aggctataggtatggcatcaag-3'	5'-gaaacaagagtgacattgggg-3'
TFG exon 5	5'-cattatttcccttgtacttttaggc-3'	5'-gggaagaacggaaagatgaag-3'
TFG exon 6	5'-cttattccttgagcttgctgg-3'	5'-caacaatgctgtaataaacacttctac-3'
TFG exon 7a	5'-ctctgtttggatggagaggg-3'	5'-ccaccagaaaactgaaatgttg-3'
TFG exon 7b	5'-acccaggttcaaggtgagtt-3'	5'-gcataccatattgcccca-3'
TFG exon 8-1	5'-gtgatggaatctaccactctgc-3'	5'-tccagcaaattatactttcaattaac-3'
TFG exon 8-2	5'-tcagggctatacccaacctg-3'	5'-ccaaacaccaataaggacttctg-3'

Table S5. Primers Used for Sequencing Exons that Were Not Covered by the Exome Analysis

COL8A1ex1F	cacctgcccataaaagcc	COL8A1ex1R	gccagagggtgacttattcc
COL8A1ex2F	gaagttaaaatgtctgacaccagg	COL8A1ex2R	atgggttgggtgaactgagg
COL8A1ex3F	cattcctattatgcaagttctcc	COL8A1ex3R	gatctgcggctttacctgtg
COL8A1ex4F	aagtcacttggccttgcag	COL8A1ex4R	cccctctgatcccataatttag
COL8A1ex5-1F	acttcattgatgtgagagacaatc	COL8A1ex5-1R	AGCCTGTCACTCCTGGTTTG
COL8A1ex5-2F	CCCAAAGGACTACCAGGACC	COL8A1ex5-2R	ACCTGGAGGGCCCATAG
COL8A1ex5-3F	TGGACCAAGAGGGGAGAAAG	COL8A1ex5-3R	CCATGAAGTCCTGCCACTC
COL8A1ex5-4F	ATTGGACCACCTGGGATTC	COL8A1ex5-4R	ACGGGCTCGTTGTTCTTG
COL8A1ex5-5F	CAGACAGGCATCTTCACCTG	COL8A1ex5-5R	ttccagtgggtacaaccaag
C3orf26iso2ex1F	ttgacacccataacccaagg	C3orf26iso2ex1R	aaattttagcaatcctaagtatgaagg
FILIP1Lex1F	ggccaaagagtggtgtcttc	FILIP1Lex1R	ttttggagagtggtgttggc
FILIP1Lex2F	agattgactttggggctgtg	FILIP1Lex2R	tctatttctgtggcagcagg
FILIP1Lex3F	ggatgaagggatatagttttgttacc	FILIP1Lex3R	gcagggctagtgcttggc
FILIP1Lex4F	gccgaattaatcaaaacaggg	FILIP1Lex4R	ggtacagtggccagctcatag
FILIP1Lex5-1F	ttgcatattgtatatgaactgacacag	FILIP1Lex5-1R	CACGTTTCCTGAGCTCTTCC
FILIP1Lex5-2F	AAAAGCTGGCAGCACTCAG	FILIP1Lex5-2R	TTGTTACTTTATTTTGCTCCACTTG
FILIP1Lex5-3F	ACTAAACTGAAAACATTAACTGTGATG	FILIP1Lex5-3R	TTGTACTTAGCAAGTTCCATTTTAAC
FILIP1Lex5-4F	AAAGCCATTGAGGATGACC	FILIP1Lex5-4R	TCGTCTTGATTCTCACTCTCCTC
FILIP1Lex5-5F	CAGAAGCAGTAGACAATGAACCAC	FILIP1Lex5-5R	CTGGGGTCTGTGCTCTGG
FILIP1Lex5-6F	AAACGCCTCCATAACACCAG	FILIP1Lex5-6R	cgagttcagtcagtcttggg
FILIP1Lex6F	tggataaaacaaaccaacacttttag	FILIP1Lex6R	ggtttcatcaaagagcagatgtc
TMEM30Cex1F	ccatccaccggctatatttc	TMEM30Cex1R	tctcacgtatggtgccaaag
TMEM30Cex2F	gcccctgacccagacag	TMEM30Cex2R	ttgcaacttagaaacaaaggagg
TMEM30Cex3F	ccataaataggctttgagttcctg	TMEM30Cex3R	cagttatcctgactacccagcc
NIT2ex1F	acttaggccgttccctttg	NIT2ex1R	cccggaagcctggaatc
TOMM70Aex1-1F	cccattccagtgctgtgc	TOMM70Aex1-1R	CATGACAAGTGTCCTCTGCC
TOMM70Aex1-2F	CTCGCTCATTGCTTTCCTTC	TOMM70Aex1-2R	gccaaggaaaagctgcac
LNP1ex1-1F	ctggccgtccttctcctc	LNP1ex1-1R	CTTCAGCGGTGAGCTCTTTC
LNP1ex1-2F	TATAGCCACGTTGGCACCTC	LNP1ex1-2R	TGAACTGAAATTACGATTTGGG
LNP1ex1-3F	GAGCTGATTTCTGCGTCAGC	LNP1ex1-3R	ttttagtctgttgctaagaaaccc
LNP1ex2F	gcctgatgatgaagtggttg	LNP1ex2R	aagagagatttctgtgggtatgag
LNP1ex3F	tgcctctgtgctaacattgc	LNP1ex3R	aaagaggacaaaaccttggg
LNP1ex4-1F	tctgattattaagagaaatgtggagtg	LNP1ex4-1R	TGGAGCAGCTACATACCCTG
LNP1ex4-2F	CCATTTCAGGATGTGGATG	LNP1ex4-2R	ccagttctccttaaatgatggc
ABI3BPex1F	gaaagggtgtgatgtcatcttg	ABI3BPex1R	tctctgcagaataactctattccc
ABI3BPex2F	ctgggaagttgggtaggatg	ABI3BPex2R	tttgtaggtcatgttacacccc
ABI3BPex3F	tgcctccaatgctggttc	ABI3BPex3R	gtctccaggggtccaaaag
ABI3BPex4F	cattttacccgaatcatggc	ABI3BPex4R	ggtgttaagtcaatgctaacagtcc
ABI3BPex5F	tcccaagttggttgaaatctg	ABI3BPex5R	ctaaagattctgaaatatcaatgctc
ABI3BPex6F	gagttgatttaggagcaaggag	ABI3BPex6R	tctccactgtttcatagctagtcag
ABI3BPex7F	gggctacttccagttctccg	ABI3BPex7R	tcgagaaaatatgtgccgtg
ABI3BPex8F	agcttcttactgcctcctatttc	ABI3BPex8R	tccagaaaagccctatcctc
ABI3BPex9F	cattttatgtcatgatgcactttc	ABI3BPex9R	tggatttcctaagaatatcagtgc

ABI3BPex10F	ttgattatgcattgagggagg	ABI3BPex10R	tcaaaatgtatttcctactggctc
ABI3BPex11F	tcctggtctttggttgcttc	ABI3BPex11R	tgagtcctgggagttatttcg
ABI3BPex12F	tggtatactgcaggcttctgg	ABI3BPex12R	tggggaaaatgaggttcatc
ABI3BPex13F	tccttcaaccagcattacaac	ABI3BPex13R	gaggatacaattttccactctgc
ABI3BPex14F	attttattcctggggccttc	ABI3BPex14R	tttggaagaaaggcattcac
ABI3BPex15F	tcatgtactcgtggcatgtg	ABI3BPex15R	tggccaacatgacttctcac
ABI3BPex16F	acctttttgtcccagtcaccc	ABI3BPex16R	cttctgggctcaagaagcac
ABI3BPex17F	tttagttcctctttagagggtgtc	ABI3BPex17R	gctggggtactggatttttcc
ABI3BPex18F	tttatttctaggttttccttctgtg	ABI3BPex18R	caaagaacttgttttcaacccc
ABI3BPex19F	gcttctagaggcttaggtactgtc	ABI3BPex19R	ttgctagaataaccccactaacc
ABI3BPex20F	tgttttaagcatgactggaagatg	ABI3BPex20R	tttcactgaagcagagtggg
ABI3BPex21F	gcttcattcatgctttctgg	ABI3BPex21R	tctaaatttcttccatatcacaacc
ABI3BPex22F	accaatctggtctggtgctg	ABI3BPex22R	ttaagggaaattcctaaaaggc
ABI3BPex23F	tgggacagaaaagagtatggg	ABI3BPex23R	tttcctgattaaaagcaaataagg
ABI3BPex24F	attcaggaggctttggtctg	ABI3BPex24R	ccccttggtgtatttggc
ABI3BPex25F	tgtacgttattactggcaactctacc	ABI3BPex25R	tgccaccaggaatgatactg
ABI3BPex26F	tctattctctgtcatccaactgc	ABI3BPex26R	tcttcagggccaacacaaac
ABI3BPex27F	tgtttataggaaacttggcagtg	ABI3BPex27R	cacccatccccaccaac
ABI3BPex28F	tgcagcaggacacaactaatg	ABI3BPex28R	tcagctgacacccagttgac
ABI3BPex29F	tcatggctttcaaccatcc	ABI3BPex29R	ttgtctcctccccaggtatg
ABI3BPex30F	tcaggagcaattaagtcagcc	ABI3BPex30R	ccttgttgtggttataacttttgc
ABI3BPex31F	aatgttgcctcctagccctc	ABI3BPex31R	tacgcaaaacattgctccac
ABI3BPex32F	tggaatgttggggttttacc	ABI3BPex32R	tgattcagattctgccatgc
ABI3BPex33F	tgatttcttgaagtatctgaccc	ABI3BPex33R	acaatgctgcaaaacattcc
ABI3BPex34F	gggtaatagagaatgaggggag	ABI3BPex34R	aattgcttgctttcctcagc
ABI3BPex35-1F	caatctatgagctgtgagggc	ABI3BPex35-1R	ACATGCTGAAGATAATTTGATCC
ABI3BPex35-2F	AGCTGGCTCCCTATTCATGG	ABI3BPex35-2R	TTGTGCTCAGACTTGACTTCAC
ABI3BPex35-3F	TGAATAGCTTTGCGGAGGAG	ABI3BPex35-3R	aatgcatttggtaatcgttgg
SENP7-F	TGCAAATCTCCTTTCAGGTC	SENP7-R	TTGCTTGAGGAACTGAAGTTTAC
RG9MTD1ex1F	aaaagcagcgccggaag	RG9MTD1ex1R	cactaagtgcatcttggaacg
RG9MTD1ex2-1F	ttggtacaaagattttaccttgtg	RG9MTD1ex2-1R	TTCCAGCCCATTGCTATGTC
RG9MTD1ex2-2F	AAAACCCTTATGGAATGTGTTTC	RG9MTD1ex2-2R	TTTTGTTACCAATTTCCCATTG
RG9MTD1ex2-3F	TTTCAGGCATGACAAAGTTTATG	RG9MTD1ex2-3R	ggcaccaccctctaggaac
ZBTB11ex1F	CTCCGACTCGTGGGTACG	ZBTB11ex1R	TAGGTAGCGGGCCGTTTTC
NFKBIZex1F	TTTTACTGGAAATCGGACGC	NFKBIZex1R	TAATTGATGGCTAAGGTGCG
TOMM70A-F	ATGCCCTCCACTGGCAGCCAG	TOMM70A-R	CTCGCTCATTGCTTTCCTTC
SENP7-ex1F	ACCGGGTCTTCGACTCCA	SENP7-ex1R	TTTTTCCTTTCCCCTCCC
SENP7-F	TGCAAATCTCCTTTCAGGTC	SENP7-R	TTGCTTGAGGAACTGAAGTTTACAG
PCNP-ex1F	ATCACATCCACTTCCGCTTC	PCNP-ex1R	TCCAGATCCGCCCATTCT
ZBTB11-ex1F	ACCCTCTCGGCTCCGCCTGG	ZBTB11-ex1R	TTTTCCTCACCTGTCCCTGA
CEP97-ex1F	CAGCTTCACATCATTAGGCG	CEP97-ex1R	CGCATCAAAAGAACTGGTCC

Table S6. Primer Sequences Used for Cloning of TFG

BamHI-TFG-f	5'-ccggatccatgaacggacagttggatct-3'
TFG-XhoI-X-NotI-r	5'-ccgcggccgcctactcgagtcgataaccaggtccaggtt-3'
TFG7b-XhoI-r	5'-ccctcgagcttgcaatgaaacctctccat-3'

Table S7. Primer Sequences Used for RT-PCR Analysis

TFGRT-6F	5'-ccacagcagccaccatatacagg-3'
TFGRT-8R	5'-ccctggaactgctgaggttgttg-3'

Table S8. Antibodies Used for Analysis

Immunohistochemistry

Antigen	Company	Dilution
TFG (rabbit polyclonal)	Protein Tech Group Inc.	1:100
ubiquitin (rabbit polyclonal)	Dako	1:2000
TDP-43 (rabbit polyclonal)	Protein Tech Group Inc.	1:3000
phosphorylated TDP-43 (pS409/410) (rabbit polyclonal)	References 14 and 15	1:3000
OPTN-C (rabbit polyclonal)	Cayman Chemical	1:500
TGN46 (sheep polyclonal)	Novus Biologicals	1:100

Immunofluorescence

Antigen	Company	Dilution
Ubiquitin (mouse monoclonal)	Millipore	1:100
TFG (rabbit polyclonal)	Protein Tech Group Inc.	1:100
TGN46 (sheep polyclonal)	Novus Biologicals	1:100

Immunocytochemistry

Antigen	Company	Dilution
TFG (rabbit polyclonal)	Abcam	1:5000
FUS (rabbit polyclonal)	Sigma-aldrich	1:1000
TDP-43 (rabbit polyclonal)	Protein Tech Group Inc.	1:3000
OPTN-C (rabbit polyclonal)	Cayman Chemical	1:500
Myc-tag (mouse monoclonal)	Life Technologies	1:5000

Table S9. Primer Sequences Used for Mutagenesis

TFG-P285L-F	5'-ctcaacaacTtcagcagttccagggatatggccag-3'
TFG-P285L-R	5'-gtccagtctgctgactatag-3'

EMBO
Molecular Medicine

Research Article
Amyloid β-proteins in CSF

Altered γ-secretase activity in mild cognitive impairment and Alzheimer's disease

Nobuto Kakuda[1,2,3], Mikio Shoji[4], Hiroyuki Arai[5], Katsutoshi Furukawa[5], Takeshi Ikeuchi[6], Kohei Akazawa[7], Mako Takami[2,3], Hiroyuki Hatsuta[8], Shigeo Murayama[8], Yasuhiro Hashimoto[9], Masakazu Miyajima[10], Hajime Arai[10], Yu Nagashima[11], Haruyasu Yamaguchi[12], Ryozo Kuwano[13], Kazuhiro Nagaike[1], Yasuo Ihara[2,14,3], the Japanese Alzheimer's Disease Neuroimaging Initiative*

Keywords: amyloid β-protein; CSF; γ-secretase; NSAID; stepwise processing

DOI 10.1002/emmm.201200214

Received December 21, 2010
Revised December 22, 2011
Accepted January 09, 2012

We investigated why the cerebrospinal fluid (CSF) concentrations of Aβ42 are lower in mild cognitive impairment (MCI) and Alzheimer's disease (AD) patients. Because Aβ38/42 and Aβ40/43 are distinct product/precursor pairs, these four species in the CSF together should faithfully reflect the status of brain γ-secretase activity, and were quantified by specific enzyme-linked immunosorbent assays in the CSF from controls and MCI/AD patients. Decreases in the levels of the precursors, Aβ42 and 43, in MCI/AD CSF tended to accompany increases in the levels of the products, Aβ38 and 40, respectively. The ratios Aβ40/43 *versus* Aβ38/42 in CSF (each representing cleavage efficiency of Aβ43 or Aβ42) were largely proportional to each other but generally higher in MCI/AD patients compared to control subjects. These data suggest that γ-secretase activity in MCI/AD patients is enhanced at the conversion of Aβ43 and 42 to Aβ40 and 38, respectively. Consequently, we measured the *in vitro* activity of raft-associated γ-secretase isolated from control as well as MCI/AD brains and found the same, significant alterations in the γ-secretase activity in MCI/AD brains.

INTRODUCTION

Senile plaques, the neuropathological hallmark of Alzheimer's disease (AD), are composed of amyloid β-protein (Aβ). Aβ is derived from β-amyloid precursor protein (APP) through sequential cleavage by β- and γ-secretases. β-Secretase cleaves at the luminal portion (β-site) of APP to generate a β-carboxyl terminal fragment of APP (βCTF), an immediate substrate of γ-secretase, to produce different Aβ species (for a review see Selkoe, 2001). The most abundant secreted Aβ species is Aβ40,

(1) Immuno-Biological Laboratories Co., Fujioka, Japan
(2) Faculty of Life and Medical Sciences, Department of Neuropathology, Doshisha University, Kyoto, Japan
(3) New Energy and Industrial Technology Development Organization (NEDO), Kanagawa, Japan
(4) Department of Neurology, Institute of Brain Science, Hirosaki University Graduate School of Medicine, Hirosaki, Japan
(5) Division of Brain Sciences, Department of Geriatrics and Gerontology, Institute of Development, Aging and Cancer, Tohoku University, Sendai, Japan
(6) Department of Neurology, Brain Research Institute, Niigata University, Niigata, Japan
(7) Department of Medical Informatics, Niigata University Medical and Dental Hospital, Niigata, Japan
(8) Department of Neuropathology, Tokyo Metropolitan Institute of Gerontology, Tokyo, Japan
(9) Department of Biochemistry, Fukushima Medical University, Fukushima, Japan
(10) Department of Neurosurgery, Juntendo University School of Medicine, Tokyo, Japan
(11) Department of Neurology, Graduate School of Medicine, University of Tokyo, Tokyo, Japan
(12) Gunma University School of Health Sciences, Maebashi, Japan
(13) Department of Molecular Genetics, Bioresource Science Branch, Center for Bioresources, Niigata University, Niigata, Japan
(14) Core Research for Evolutional Science and Technology (CREST), Japan Science and Technology Corporation, Tokyo, Japan
***Corresponding author:** Tel: +81 774 656058; Fax: +81 774 731922; E-mail: yihara@mail.doshisha.ac.jp

whereas the species that has two extra residues (Aβ42) is a minor one (<10%); however, the latter is the one that deposits first and predominates in senile plaques (Iwatsubo et al, 1994).

Presenilin 1/2 make up the catalytic site of γ-secretase. The enzymatic properties of γ-secretase that cleave the transmembrane domain of βCTF have been an enigma, although recent studies provided partial elucidation of this mechanism (Qi-Takahara et al, 2005; Takami et al, 2009). γ-Secretase has two product lines, which successively convert the Aβ49 and Aβ48 that are generated by ε-cleavage, to shorter Aβs by releasing tri- or tetrapeptides in a stepwise fashion. Aβ49 is successively cleaved mostly into Aβ40 via Aβ46 and Aβ43, while Aβ48 is similarly cleaved into Aβ38 via Aβ45 and Aβ42 (see Fig 1). Importantly, the differences between the amounts of released tri- and tetrapeptides determine the levels of the different Aβ species produced (Takami et al, 2009). Thus, the true activity of γ-secretase is defined by the amounts of tri- and tetrapeptides released, but not by the amounts of Aβ species produced. Of note, the most abundant species Aβ40 is derived not from Aβ42, but from Aβ43. Also Aβ38 is derived mainly from Aβ42 (Fig 1). The longer Aβs in cerebrospinal fluid (CSF) including Aβ49 and 46 as well as Aβ48 and 45 must be generated at negligible levels, but may neither be secreted to the interstitial fluid (ISF) nor recruited to CSF. This suggests that the status of brain, and possibly neuronal, γ-secretase could be accurately assessed by measuring all four Aβ species generated by the two product lines of γ-secretase.

Using enzyme-linked immunosorbent assays (ELISAs), we quantified Aβ40 and 43 and Aβ38 and 42 in CSF samples from control subjects and mild cognitive impairment (MCI)/AD patients. The CSF concentrations of Aβ43 and Aβ42 were found to be significantly lower in MCI/AD compared with controls. The ratio of Aβ38/42, which represents the ratio of product/precursor and thus the cleavage efficiency of Aβ42, was plotted against the ratio of Aβ40/43, which represents the ratio of product/precursor in the other product line and thus the cleavage efficiency of Aβ43. The ratio of Aβ38/42 was largely proportional to that of Aβ40/43, indicating that the two cleavage processes are tightly coupled, but both were generally higher in MCI/AD patients compared to control subjects These results

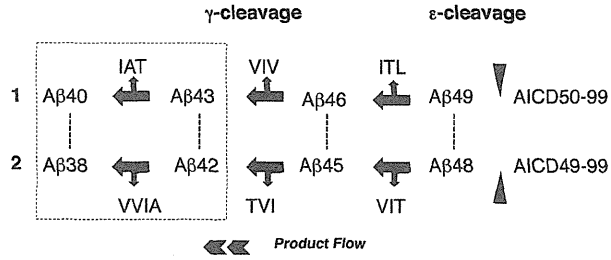

Figure 1. Generation of Aβs through stepwise processing of βCTF. At the first step, βCTF is cleaved at the membrane-cytoplasmic boundary (ε-cleavage), producing AICD (APP intracellular domain) 50–99 and 49–99. Counterparts Aβ49 and 48 in turn are cleaved in a stepwise fashion, releasing tri- and tetrapeptides. One product line converts Aβ49 mostly to Aβ40 via Aβ46 and Aβ43. The other product line converts Aβ48 to Aβ38 via Aβ45 and Aβ42. It should be noted that the differences between the amounts of released tri- or tetrapeptide determine the amounts of Aβs produced. Broken lines indicate corresponding Aβs on the two product lines.

suggest that the activity of brain γ-secretase in MCI/AD is enhanced at the conversion of Aβ43 to Aβ40 and Aβ42 to Aβ38, which would result in significantly lower CSF concentrations of Aβ42 and 43. In support of this hypothesis, the activities of raft-associated γ-secretase from control and MCI/AD brains were found to be significantly different: although the total Aβ production was similar, the γ-secretase in MCI/AD brains produced significantly larger ratios of Aβ40/43 and Aβ38/42 than the enzyme in control brains. This raises the possibility that lower CSF levels of Aβ42 and 43 simply reflect the altered γ-secretase activity in the MCI/AD-affected brains.

RESULTS

The CSF concentrations of Aβs were in the following order: Aβ40 > Aβ38 > Aβ42 ≫ Aβ43 in all CSF samples examined (Table 1 and Supporting Information Fig S2A). The relative amounts of Aβs were constant across the samples: Aβ38:40 ratio in CSF was ~1:3, and Aβ42:43 ratio was ~10:1. The CSF

Table 1. Subject characteristics and CSF concentrations of Aβs

	Control	MCI	AD	ANOVA ***p-value
Age (years)	74.9 ± 7.5	72.5 ± 6.6	72.3 ± 8.2	
N (male/female)	21 (10/11)	19 (7/12)	24 (7/17)	
MMSE score	28.7 ± 1.9	25.7 ± 2.6	19.6 ± 3.3	
ApoE ε4	3 (14.3%)	10 (52.6%) [a]	14 (58.6%) [a]	
Aβ38 (pM)	594.5 ± 286.3	669.4 ± 247.6	760.57 ± 269.4	
Ln(Aβ38)	6.28 ± 0.46	6.44 ± 0.38	6.56 ± 0.41	NS
Aβ40 (pM)	1607.9 ± 712.9	1939.5 ± 698.0	2292.6 ± 799.6	
Ln(Aβ40)	7.28 ± 0.47	7.51 ± 0.38	7.68 ± 0.35	0.007
Aβ42 (pM)	133.1 ± 53.4	83.2 ± 49.4**	90.3 ± 40.1 [a]	
Ln(Aβ42)	4.80 ± 0.47	4.25 ± 0.60	4.40 ± 0.47	0.004
Aβ43 (pM)	11.8 ± 5.7	6.8 ± 5.6**	7.0 ± 4.6**	
Ln(Aβ43)	2.32 ± 0.60	1.59 ± 0.86	1.76 ± 0.62	0.004

[a]2 MCI subjects were homozygous for ε4, while 4 AD subjects were homozygous for the allele.
**$p < 0.05$; Dunnett's *t*-test after log-transformation for comparing between control and MCI or AD.
***p-value of analysis of variance after log-transformation.

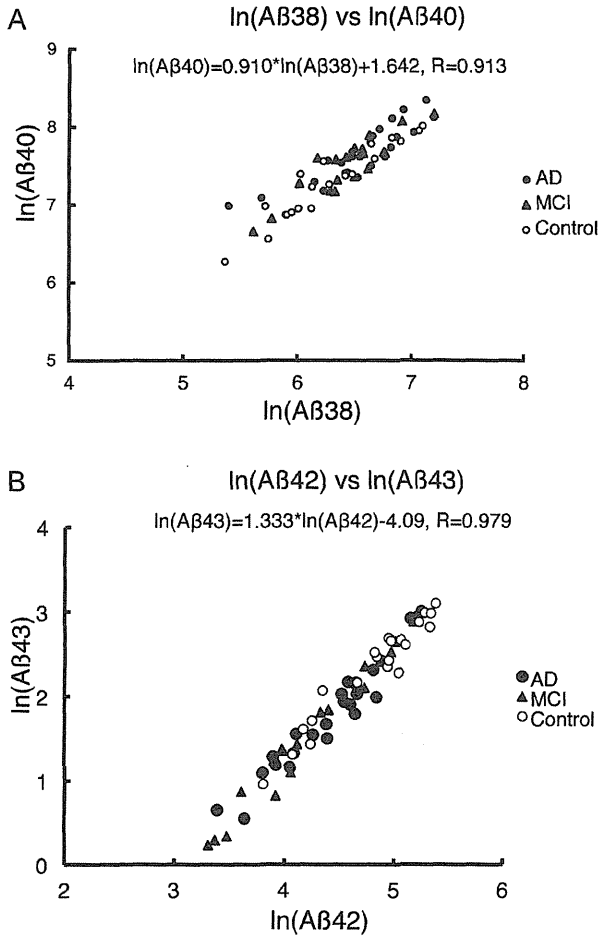

Figure 2. Relationships between the levels of Aβ40 and 38, and between those of Aβ43 and 42 in CSF from controls and MCI/AD patients.

A. The levels of ln(Aβ40) were proportional to those of ln(Aβ38) ($\ln(A\beta40) = 0.910 \times \ln(A\beta38) + 1.642$, $R = 0.913$).

B. The levels of ln(Aβ43) were proportional to those of ln(Aβ42) ($\ln(A\beta43) = 1.333 \times \ln(A\beta42) - 4.09$, $R = 0.979$). It should be noted that the levels of both ln(Aβ42) and ln(Aβ43) in MCI [filled triangle ($n = 19$)]/AD [filled circle ($n = 24$)] are lower than those in controls [open circles ($n = 21$)].

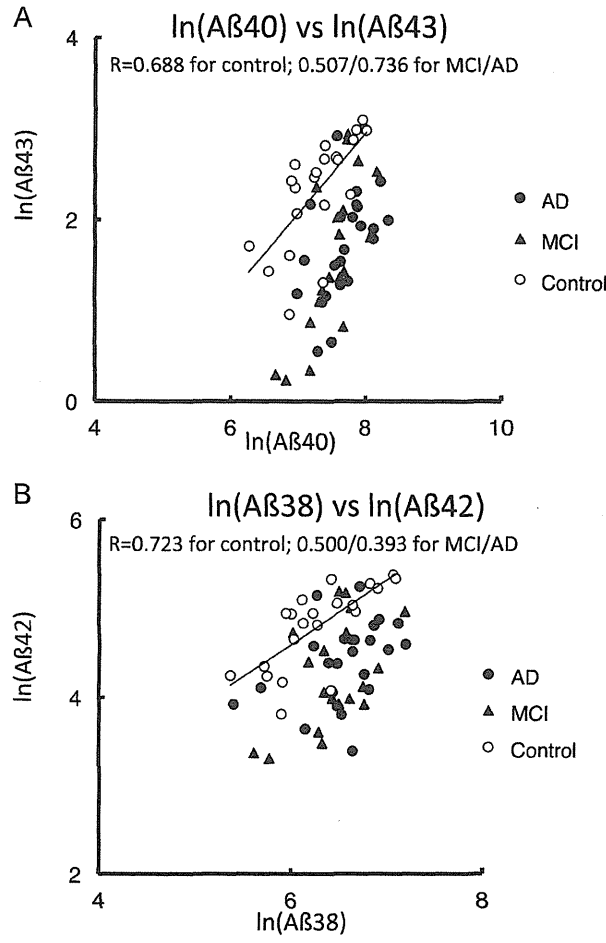

Figure 3. Relationships between the levels of Aβ43 and 40, and between those of Aβ42 and 38 in CSF from controls (open circles) and MCI (closed triangle)/AD patients (closed circle).

A. The levels of ln(Aβ43) correlate with those of ln(Aβ40) within controls ($R = 0.688$), and barely within MCI/AD subjects ($R = 0.507/0.736$). The plots for MCI/AD were located below the regression line for control ($p < 0.001$, ANOVA).

B. The levels of Aβ42 correlate with those of Aβ38 within controls ($R = 0.723$), and barely within MCI/AD ($R = 0.500/0.393$). The plots for MCI/AD were situated below the regression line for controls ($p < 0.001$, ANOVA).

concentrations of Aβ40 were significantly increased in AD compared to control (Table 1; $p < 0.05$, Dunnett's t-test). Additionally, the CSF concentrations of Aβ38 tended to be increased in AD patients compared to controls. In contrast, those of Aβ42 and 43 were significantly decreased in MCI/AD compared to controls ($p < 0.05$, Dunnett's t-test). Interestingly, as reported previously (Schoonenboom et al, 2005), the CSF concentrations of Aβ40 and Aβ38 were proportional to each other in all subjects [Fig 2A; $\ln(A\beta40) = 0.910 \times \ln(A\beta38) + 1.642$, $R = 0.913$, where ln(Aβ40) is the logarithm of Aβ40], even in MCI/AD cases. This was despite the fact that these species are derived from and the final products of the two different product lines of γ-secretase activity (Fig 1; Takami et al, 2009). In other words, the amounts of products in the third step of cleavage were strictly proportional to each other across the product lines.

Aβ42 and Aβ43 are produced by the second cleavage step of each product line. Like Aβ40 and Aβ38, the CSF concentrations of Aβ42 and Aβ43 are also proportional to each other in controls and in MCI/AD patients [Fig 2B; $\ln(A\beta43) = 1.333 \times \ln(A\beta42) - 4.09$, $R = 0.979$]. On the other hand, the levels of Aβ43 and Aβ40 (a precursor and its product) were correlated in control [Fig 3A; $\ln(A\beta43) = 0.884 \times \ln(A\beta40) - 4.118$, $R = 0.688$] and in MCI/AD subjects ($R = 0.507/0.736$ for MCI/AD, respectively) but the MCI/AD values were located below the regression line for controls and thus provided lower Aβ43 measures compared with controls for a given Aβ40 measure (Fig 3A; $p < 0.001$, analysis of variance, ANOVA). Conversely,

for a given Aβ43 value, the plot provided a higher Aβ40 measure in MCI/AD cases. There was a similar situation for the levels of Aβ42 and Aβ38. The levels of Aβ42 and Aβ38 were correlated each other in control subjects [Fig 3B; $\ln(A\beta42) = 0.724 \times \ln(A\beta38) + 0.251$, $R = 0.723$], but barely in MCI/AD ($R = 0.500$ for MCI; 0.393 for AD), and the MCI/AD plots were situated below the regression line for controls ($p < 0.001$, ANOVA). For a given Aβ42 value, the plot provided a higher Aβ38 measure in MCI/AD compared with controls.

These lower concentrations of Aβ42 appeared to be compensated with higher concentrations of Aβ38 as the levels of $\ln(A\beta38 + A\beta42)$ did not vary even in MCI/AD ($p = 0.293$, ANOVA). Thus, this points to the possibility that more Aβ42 and Aβ43 are converted to Aβ38 and Aβ40, respectively, in MCI/AD brains. According to numerical simulation based on the stepwise processing model, as the levels of βCTF decline to null, the levels of Aβ43 and 42 decrease and the ratios of Aβ40/43 and Aβ38/42 increase (unpublished observation). However, this situation can be excluded as the mechanism for lower concentrations of Aβ42 and 43, because the levels of βCTF have never been reported to be reduced in AD brains nor in plaque-forming Tg2576 mice that show lower CSF Aβ42 concentrations (Kawarabayashi et al, 2001). Thus, it is reasonable to suspect that the final cleavage steps from Aβ43 mostly to 40 and from Aβ42 to 38 are significantly enhanced in parallel (increases in released tri- and tetrapeptides) in brains affected by MCI/AD compared with controls (Fig 1).

This relationship in γ-secretase cleavage becomes clearer by plotting the product/precursor ratio representing cleavage efficiency at the step from Aβ42 to 38 (Aβ38/42) against that representing the cleavage efficiency at the step from Aβ43 to 40 (Aβ40/43) (Fig 4). The 'apparent' cleavage efficiency of Aβ43 was approximately 40-fold larger than that of Aβ42. The two ratios in CSF samples from MCI/AD and control subjects were largely proportional to each other, indicating that the corresponding cleavage processes in the two lines are tightly coupled (Fig 4). All plots were situated on a distinct line [$\ln(A\beta38/42) = 0.748 \times \ln(A\beta40/43) - 2.244$, $R = 0.936$] and its close surroundings. An increase in the cleavage from Aβ43 to 40 (*i.e.* more Aβ43 is converted to Aβ40) accompanied an increase in the cleavage from Aβ42 to 38 and *vice versa*, although the mechanism underlying this coupling between the two product lines remains unknown. This reminds us of the 'NSAID effect' in the 3-([3-cholamidopropyl]dimetylammonio)-2-hydroxy-1-propanesulfonate (CHAPSO)-reconstituted γ-secretase system (Takami et al, 2009; Weggen et al, 2001) in which the addition of sulindac sulfide to the γ-secretase reaction mixture, as expected, significantly suppressed Aβ42 production and increased Aβ38 production presumably by increasing the amounts of released tetrapeptide (VVIA) (Takami et al, 2009) and other peptides.

Most importantly, this graph provides a clear distinction between the control and MCI/AD groups (Fig 4; Aβ40/43 for MCI/AD *vs.* control, $p = 0.000$; Aβ38/42 for MCI/AD *vs.* control, $p = 0.000$; ANOVA, followed by Dunnett's *t*-test). The control values plotted close to the origin, whereas those for MCI/AD patients were distant from the origin along the line [$\ln(A\beta38/42) = 0.748 \times \ln(A\beta40/43) - 2.244$, $R = 0.936$]. It is also of note

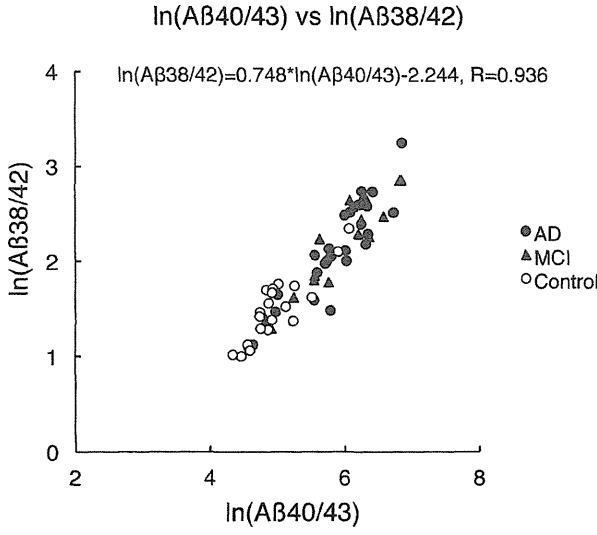

Figure 4. Ln(Aβ40/43) *versus* ln(Aβ38/42) plot. The ratios represent the cleavage efficiency at the final step of each line. Both ratios are largely proportional to each other ($y = 0.748 \times -2.244$, $R = 0.936$) and plots are located on the line and its close surroundings. This plot clearly distinguishes between control subjects and MCI/AD patients (Aβ40/43 for MCI *vs.* control, $p = 0.000$; Aβ38/42 for MCI *vs.* control, $p = 0.000$; ANOVA, followed by Dunnett's *t*-test). Control plots [open circles ($n = 21$)] are located close to the origin and MCI/AD plots [closed triangles ($n = 19$) and closed circles ($n = 24$), respectively] are a little distant from the origin.

that there was no significant difference between MCI and AD patients (Fig 4; Aβ40/43 for AD *vs.* MCI, $p = 1.000$; Aβ38/42 for AD *vs.* MCI, $p = 1.000$; Bonferroni's *t*-test). Two control values were a little farther from the origin, which may suggest that these subjects already have latent Aβ deposition or are in the preclinical AD stage. Additionally, we examined quite a small number of CSF samples from presenilin (PS) 1-mutated (symptomatic) familial AD (FAD) patients (T116N, L173F, G209R, L286V and L381V). Out of the three FAD cases near the regression line, two (T116N and L286V) were distant from the origin like sporadic AD cases and one (L381V) was closer to the origin than controls (both Aβ42/43 levels were lower than control; unpublished data). The remaining two (G209R and L173F) were extremely displaced from the line. Thus, a larger number of FAD cases are needed to give an appropriate explanation for their unusual characteristics in the plot, and the alteration of CSF Aβs shown above seems to be applicable only for sporadic AD.

Altogether, in MCI/AD, more Aβ42 and 43 are processed to Aβ38 and 40, respectively, than in controls. Even in MCI/AD, strict relationships are maintained between the levels of Aβ42 and Aβ43, and between those of Aβ38 and Aβ40 as seen in controls, which are predicted by the stepwise processing kinetics (unpublished observation). Thus, our observations suggest that lower CSF concentrations of Aβ42 and 43 and presumably higher CSF concentrations of Aβ38 and 40 are the consequence of altered γ-secretase activity in brain rather than the effect of preferential deposition of the two longer Aβ species (Aβ42 and 43) in senile plaques, which would not have maintained such strict relationships between the four Aβ species in CSF.

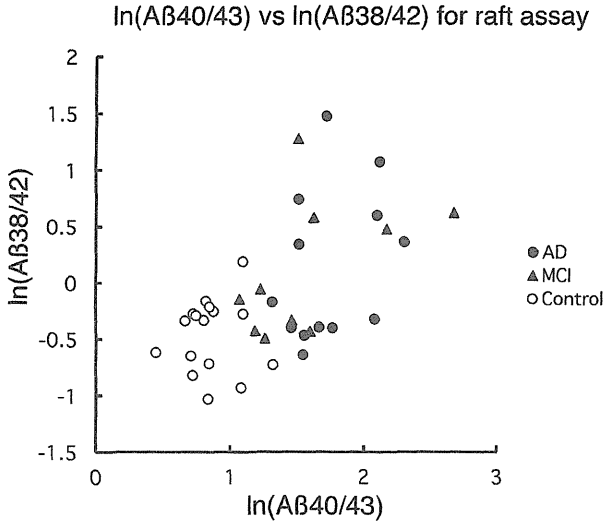

Figure 5. Ln(Aβ40/43) *versus* ln(Aβ38/42) plot based on direct quantification of raft-associated γ-secretase activity. The raft-associated γ-secretase prepared from control and MCI/AD brain specimens was incubated with βCTF for 2 h at 37°C (see Materials and Methods Section). Produced Aβs were quantified by Western blotting using specific antibodies. This plot distinguishes between control subjects and MCI/AD patients (Aβ40/43 for control *vs.* MCI/AD, $p < 0.001$; Aβ38/42 for control *vs.* MCI/AD, $p = 0.001$; Welch's *t*-test). MCI/AD plots [closed triangles ($n = 10$) and closed circles ($n = 13$), respectively] are as a whole a little distant from the origin, whereas control plots [open circles ($n = 16$)] are close to the origin.

To further test our hypothesis, we directly measured γ-secretase activities associated with lipid rafts isolated from AD, MCI and control cortices (Brodmann areas 9–11). For definite confirmation of the Aβ species, the reaction mixtures were subjected to quantitative Western blotting using specific antibodies rather than ELISA. At time 0, deposited Aβ42/43 species were detected in rafts from MCI/AD brains but not in control specimen (Supporting Information Fig S3). The amounts of ln(Aβ38 + Aβ42), which reflect the total capacity of the Aβ38/42-producing line, did not vary between AD, MCI and controls (Supporting Information Fig S4; $p = 0.969$, ANOVA). Thus, the gross activities of raft γ-secretase were comparable among the three groups. However, the plotted values for Aβ40/43 *versus* Aβ38/42 are divided into two groups: MCI/AD and controls (Fig 5; Aβ40/43 for control *vs.* MCI/AD, $p < 0.001$; Aβ38/42 for control *vs.* MCI/AD, $p = 0.001$; Welch's *t*-test) in the same way as those derived from CSF (Fig 4). It is notable that Figs. 4 and 5 are based on different methods, ELISA and Western blotting, respectively, but give similar results. There were no significant differences between MCI and AD specimen, although MCI patients (91 ± 4.9-year-old) were older than controls (77 ± 6.5-year-old) or AD patients (80 ± 5.0-year-old) (Aβ40/43 for MCI *vs.* AD, $p = 0.342$; Aβ38/42 for MCI *vs.* AD, $p = 0.911$). There were similar significant differences between control *versus* AD in the groups of which the ages were not significantly different (Aβ40/43 for control *vs.* AD, $p < 0.001$; Aβ38/42 for control *vs.* AD, $p = 0.03$).

DISCUSSION

Here, we assume that (i) Aβs in CSF are produced exclusively by γ-secretase in the brain, possibly in neurons; and (ii) Aβs in CSF are in the steady state. With these assumptions, the combined measurement of four Aβ species in CSF should predict the activity of γ-secretase in the brain. Here, the alterations in the γ-secretase activities do not mean the gross activity, *i.e.* total Aβ production, but the cleavage efficiency of the intermediates, Aβ42 and Aβ43.

In the present study, we quantified in CSF the four Aβ species, Aβ38/42 and Aβ40/43, but the Western blotting indicated the presence of additional Aβ species, Aβ37 and 39, in CSF (Supporting Information Fig S2). At present, we cannot exclude the possibility that a certain carboxyl terminus-specific protease(s) in CSF acts on the pre-existing Aβ species and converts them to Aβ37 and 39 (Zou et al, 2007). However, according to our unpublished data (Takami et al, unpublished observations), it is plausible that Aβ37 is derived from Aβ40, whereas Aβ39 is derived from Aβ42. Even if so, these pathways are very minor (~20–100-fold less) compared to the two major pathways, Aβ42 to Aβ38, and Aβ43 to Aβ40, when assessed by a reconstituted system (Takami et al, 2009). Thus, such strict relationships between four Aβs may have been relatively independent of Aβ37 and 39. The detailed relationship between all Aβs in the CSF awaits further quantification of the additional two Aβ species.

Currently, we do not know why the observation that Aβ40 is higher in MCI/AD CSF has so far not been reported except a recent paper (Simonsen et al, 2007). In fact, some of us previously reported no significant differences in CSF Aβ40 between AD and control subjects using a different ELISA (Shoji et al, 1998). It may be notable that we used newly constructed ELISA for Aβ40 based on a different set of monoclonal antibodies and thus, those discrepancies may come from the different antibody/epitope combination used for ELISA and/or different assay methods. In particular, it should be noted that all ELISAs used here detect Aβ1-x only, but not amino-terminally truncated forms. In this context, the ratio of Aβ40/43 appears to be more informative to discriminate between control and MCI/AD than the absolute levels of Aβ40 alone (Table 1 and Fig 5). It is possible that even if Aβ40 is not different between control and MCI/AD, the ratio Aβ40/43 could discriminate them.

We are the first to measure CSF Aβ43 using ELISA. The CSF concentrations of Aβ43 are 10-fold less than those of Aβ42. Nevertheless, the specificity of the newly constructed ELISA made the quantification of accurate levels of Aβ43 possible (Supporting Information Fig S1). Regarding the Aβ43 measures, we observed that its behaviour is entirely similar to that of Aβ42 in MCI/AD. Our preliminary observations using immunocytochemistry and ELISA quantification strongly suggest that Aβ43 deposits in aged human brains at the same time as Aβ42 (unpublished observations). Furthermore, Saido and colleagues have only recently reported that a PS1 R278I mutation in mice (heterozygous) caused an elevation of Aβ43 and its early and pronounced accumulation in the brain (Saito et al, 2011). It is possible that the cleavage of βCTF by this R278I γ-secretase may

be profoundly suppressed in the third cleavage step of the product line 1 (see Fig 1), which would result in negligible levels of Aβ40 and unusually high levels of Aβ43 (Nakaya et al, 2005). These results suggest that the role of Aβ43 should be reconsidered for the initiation of β-amyloid deposition and thus in AD pathogenesis.

Lower CSF concentrations of Aβ42 and 43 are not exclusively limited to MCI/AD. For example, similar low concentrations of Aβ42 and 43 were found in the CSF from eight patients with idiopathic normal pressure hydrocephalus (iNPH) (Aβ42, 76.3 ± 37.3 pM, $p = 0.012$ compared to controls: Aβ43, 5.2 ± 2.9 pM, $n = 8$, $p = 0.004$ compared to controls: Bonferroni's *t*-test; Silverberg et al, 2003). Thus, lower CSF concentrations of Aβ42 and 43 alone were unable to distinguish between iNPH and MCI/AD, and further, it is claimed that the former is often associated with abundant senile plaques, raising the possibility that Aβ deposition is enhanced by iNPH (Silverberg et al, 2003). However, when their partners Aβ38 and 40 were measured in CSF, both were found not to be significantly increased in iNPH (Aβ38, 459.2 ± 138.5 pM, $p = 0.484$ compared to controls; Aβ40, 1094.4 ± 375.3 pM, $n = 8$, $p = 0.103$ compared to controls; Table 1) in sharp contrast to MCI/AD indicating that the cleavage in iNPH at the steps from Aβ43 to 40 and from Aβ42 to 38 is not enhanced as it is in MCI/AD. Thus, it may be that the dilution effect elicited by ventricular enlargement would be the cause of lower CSF Aβ42 and 43 found in iNPH.

Currently, we do not know the mechanism behind the altered activity of brain γ-secretase in MCI/AD (Fig 4). First, it is of note that rafts prepared from MCI/AD brains but never from control brains at SP stage 0/A accumulated Aβ42 and Aβ43 (Supporting Information Fig S3; Oshima et al, 2001). It is possible that raft-deposited Aβ42/43 could induce a change in the γ-secretase activity, although the extent of the alteration in the activity appears not to be related to the extent of accumulation (unpublished observation). In this regard, it is of interest to note that Tg2576 mice, the best characterized AD animal model, shows reduced levels of Aβ42 in plasma as well as in CSF at the initial stage of Aβ deposition (Kawarabayashi et al, 2001). If the assumption here is correct, this may suggest that γ-secretase that produces plasma Aβs could also be altered. However, thus far, we have failed to replicate significantly lower Aβ42 levels or Aβ42/Aβ40 ratios in plasma from AD patients.

Second, there could be heterogenous populations of γ-secretase complexes that have distinct activities due to subtle differences in their components. γ-Secretase is a complex of four membrane proteins including PS, nicastrin (NCT), anterior pharynx defective 1 (Aph1) and presenilin enhancer 2 (Pen 2) (Takasugi et al, 2003). Aph 1 has three isoforms, and each can assemble active γ-secretase together with other components (Serneels et al, 2009). NCT, a glycoprotein, is present in immature and mature forms (Yang et al, 2002). The abundance of these heterogenous populations of proteins in the brain is probably under strict control. During MCI/AD, a certain population could replace other populations of γ-secretase and thus may show a distinct activity as a whole.

The data shown here represent only a cross-sectional study, but our keen interest is how the CSF levels of the four Aβ species would shift during the longitudinal course in an individual who is going to develop sporadic AD. Does one have any period during life when Aβ42 and 43 are at higher levels in CSF, and thus the ratios of Aβ38/42 and Aβ40/43 are smaller? At this period when the final cleavage steps of γ-secretase would be suppressed, the ISF concentrations of Aβ43 and 42 would increase, which would start or promote their aggregation in the brain parenchyma. If so, during life span, the individual's plot would move down along the regression line and move up as senile plaques accumulate, and the individual would eventually develop sporadic AD. However, thus far the period when there are increases in CSF Aβ42/43 has never been reported for sporadic AD. Nor has it been reported for asymptomatic FAD carriers (Ringman et al, 2008), whereas their plasma is known to contain higher levels (and percent) of Aβ42 (Kosaka et al, 1997; Ringman et al, 2008; Scheuner et al, 1996). It is likely that the stage of normal cognition and Aβ accumulation already accompanies reduced CSF Aβ42. If so, the alterations of γ-secretase should continue on for decades. Most interestingly, this alteration of CSF Aβ regulation seems to be planned to prevent further accumulation of Aβ42 and 43 in the brain.

However, Hong et al (2011) have recently shown, using *in vivo* microdialysis to measure ISF Aβ in APP transgenic mice, that the increasing parenchymal Aβ is closely correlated with decreasing ISF Aβ, suggesting that produced Aβ42 is preferentially incorporated into existing plaque-Aβ. This is a prevailing way of the interpretation of the data. Another way of the interpretation of data would be that during aging from 3 to 24 months, γ-secretase activity becomes altered and produces decreasing amounts of Aβ but with an increasing ratio of Aβ38/42 (and Aβ40/43). It is worth to mention that produced Aβ42 (but not Aβ40) appears to be selectively bound to rafts (from CHO cells) after long incubation (>4 h; Wada et al, unpublished observation). Also of note is that we quantified the total (free and bound) Aβ produced by an *in vitro* reconstituted system (Fig 5). What is claimed here is that decreased levels of CSF Aβ42 are largely due to alterations of γ-secretase activity rather than due to selective deposition of Aβ42 in preexisting plaques. What proportions of decreased ISF (CSF) Aβ42 levels would be contributed to by altered γ-secretase activity and selective deposition of Aβ42/43 to parenchymal plaques awaits future studies.

Finally, our observation has therapeutic implication. As shown elsewhere and here above, if Aβ42 is the culprit for MCI/AD, non-steroidal anti-inflammatory drugs (NSAIDs) would have been quite a reasonable therapeutic compound, which enhances cleavage at the third step in the stepwise processing, leading to lower levels of Aβ42 without greatly interfering with the Aβ bulk flow (Weggen et al, 2001). This sharply contrasts with some of the γ-secretase inhibitors currently under development and in clinical trial, which block the Aβ bulk flow. However, the present study raises the possibility that even if NSAIDs are administered, the expected beneficial effect could be minimal in MCI/AD patients, because in these patient brains, γ-secretase is already shifted to an NSAID-like effect.

